Proceedings of the ASME 2010 3rd Joint US-European Fluids Engineering Summer Meeting and 8th International Conference on Nanochannels, Microchannels, and Minichannels
FEDSM-ICNMM2010
August 1-5, 2010, Montreal, Canada

FEDSM-ICNMM2010-30028

FlUID-STRUCTURE INTERACTION IN ANNULAR FlOWS WITH SEVERAL MODES OF VIBRATION

Dr. Abolghasem Mekanik
Department of Mechanical Engineering,
Bu-Ali Sina University, Hamedan, Iran
Email: Meka47ir@yahoo.com

Prof. Naser Sayma
Thermo-Fluid Mechanics Research Centre
Sussex University, Brighton BN1 9QT, UK
Email: A.sayma@sussex.ac.uk

ABSTRACT
This paper describes two accurate Flow-Induced Vibration (FIV) methods used to analyze the induced vibrations caused by the laminar fluid flows in uniform annular geometries. In both methods, the uniform annuli which are composed of two concentric cylinders are considered. The outer cylinder is set on translational oscillation without or with a predetermined mode of vibration and with a known initial velocity. In the first method, the small amplitude motion of the outer cylinder is used to analyze the problem considered by using the direct coupling of the fluid and structure through the accurate simultaneous solution of the Navier-Stokes and structural equations. In the computational domain, the problem has been solved using an accurate time-integration method based on a finite-difference formulation and primitive variables. In this method, the real-time discretization of the Navier-Stokes equations for unsteady incompressible flows is based on a three-time-level implicit scheme. A pseudo-time integration with artificial compressibility is then introduced to advance the solution to a new real-time level. An implicit Euler scheme is used for the pseudo-time discretization, and the finite-difference spatial discretization is based on a stretched staggered grid. In the second method, the Reynolds-averaged Navier-Stokes equations are used to represent the unsteady flow in a nonlinear time-accurate fashion. In this case, the structural model is based on a linear modal model. The fluid mesh is moved at each time-step according to the structural motion, so that the changes in fluid-dynamic damping and flow unsteadiness can be accommodated. Based on the second approach, a code named SURF was generated to handle the solution from the steady state solution till the unsteady one which is in the form of vibratory motion of the outer cylinder. In this way the stability analyses can be performed for the structure by using several modes of vibration of the structure *vis-à-vis* to the first method in which only translational motion of the outer cylinder is taken into account. The stability of the outer cylinder assessed by two methods in terms of the damped oscillation of the cylinder represents the decay in the amplitudes of vibration due to the fluid added damping. The results of this research can be used for the FIV and FSI analyses of the annular flows which could be found in many industries.

INTRODUCTION
Cylindrical structures subjected to either internal, external or annular flows are found in many engineering constructions, particularly in most of the chemical industries in the form of piping of all kinds, marine risers, chimneys, fuel pins and control rods in nuclear reactors, heat exchanger tube arrays, thin walled shrouds and flow-containment shells in nuclear reactors, aircraft engines, and jet pumps; to name but a few most familiar such systems. A review of the work done in this field is given in references (Paidoussis 1998, 2003).

The instabilities associated with internal and external axial flows are of limited practical concern for conventional engineering systems. This is not the case with instabilities associated with annular flows. Cylindrical structures subjected to annular flow were found to develop very severe flow-induced vibrations and instabilities in many engineering applications. As a result, increasing effort has recently been devoted to the study of flow-induced vibrations of these systems in narrow annular flows (Mateescu et al. 1985 -1988, Parking et al. 1984).

By using a simplified unsteady viscous analysis in laminar annular flows past oscillating cylinders, it was found (Mateecsu et al. 1987) that the unsteady viscous effects have an increased influence on the system stability when the annular gap becomes narrower, which is the case in many engineering applications. However, in many other engineering applications the annular flow is turbulent, and hence an unsteady turbulent flow analysis is required to be used in the study of flow-induced vibrations of such systems, a case which is considered as an extension to the present investigation and will be presented in the future work using the second approach.

To solve the laminar flow cases, two computational methods have recently been developed for the accurate integration of the Navier-Stokes equations, applicable to unsteady flows with oscillating boundaries in more realistic and complex geometric configurations: (i) a time-integration method based on a finite-difference formulation and artificial compressibility (Mateescu *et al* . 1991, 1994a, b, c) used for small amplitude oscillations, and (ii) a method based on the time-dependent coordinate transformation (TDCT) which is more accurate for larger amplitude oscillations practically found in the real applications (Mekanik *et al.* 1993, 2007).

In many cases, the amplitudes of vibration are not small with respect to the annular gap, and hence the effect of nonlinearities on the unsteady pressures and on the unsteady fluid-dynamic forces cannot be ignored. Moreover, the nonlinear unsteady fluid forces depend on both the displacement and the velocity of the oscillating structural boundary, in agreement with physical reality, but in contrast with the linear ones calculated based on the small amplitude assumption, which are only velocity-dependent. As a result of nonlinear effects, the fluid-added mass and viscous damping (which are proportional to the real and imaginary components of the unsteady fluid forces) may substantially change, thus modifying considerably the dynamic behaviour of the system in terms of changes in coupled (fluid-structure) damping and frequency of oscillation.

An accurate nonlinear solution for the unsteady flows in the case of larger amplitudes of oscillation is also important for the study of the dynamics of fluidelastic systems beyond the first loss of stability, which is not only of academic, but also of practical interest. Hence, there is need to find more accurate nonlinear solution capable of handling large amplitude oscillations as well as considering the turbulent cases, which are required for solving unsteady flow problems encountered in engineering applications .

In response to this need, this paper presents (i) the new formulation for unsteady annular flows based on mean position analysis, capable of solving accurately the problem in the case of small-amplitude oscillations of the solid boundaries, (ii) using the SURF Code to obtain the comparable results with the results of case (i), and (iii) using the same Code to investigate the case of much higher amplitudes of oscillation as well as investigating the cases of turbulent flows. This last objective will be the future extension of the present work.

In the fixed-boundary computational domain obtained as a result of mean position analysis, the boundary conditions on the oscillating walls are rigorously implemented. In this computational domain, the problem has been solved using an accurate time-integration method based on a finite-difference formulation and primitive variables (Mekanik 1993). In subsequent sections, the mean position method (MP) is explained followed by the method used by the SURF Code.

FIRST METHOD: MEAN POSITION ANALYSIS FORMULATION

For the configuration shown in Fig. 1, the incompressible time-dependent Navier–Stokes and continuity equations in 3-D cylindrical coordinates can be expressed in nondimensional conservation-law form with respect to a reference velocity U_o and annular gap h width as

$$\frac{\partial \mathbf{V}}{\partial t}+\mathbf{Q}(\mathbf{V},p)=\mathbf{0},\ \ \nabla\cdot\mathbf{V}=\frac{\partial u}{\partial x}+\frac{\partial v}{\partial r}+\frac{1}{r}\frac{\partial w}{\partial \theta}=0 \tag{1}$$

where $\mathbf{V}=[u,v,w]^{\mathrm{T}}$ is the nondimensional velocity vector, and the vector $\mathbf{Q}(\mathbf{V},p)$, which includes the convective derivative, pressure and viscous terms, has for example component $Q_u(u,v,w,p)$ expressed as

$$Q_u(u,v,w,p)=\frac{\partial(uu)}{\partial x}+\frac{1}{r}\frac{\partial(rvu)}{\partial r}+\frac{1}{r}\frac{\partial(wu)}{\partial \theta}$$
$$+\frac{\partial p}{\partial x}-\frac{1}{\mathrm{Re}}\left[\frac{\partial^2 u}{\partial x^2}+\frac{1}{r}\frac{\partial}{\partial r}\left(r\frac{\partial u}{\partial r}\right)+\frac{1}{r^2}\frac{\partial^2 u}{\partial\theta^2}\right], \tag{2}$$

in which $\mathrm{Re}=U_o h/\nu=\mathrm{Re}_H/2$, where Re_H represents the Reynolds number based on the hydraulic diameter of the annular passage, $D_H=2h$ (for nomenclatures see Fig. 1).

These governing equations are subjected to the following boundary conditions:

$$u=0,\qquad v=\dot{e}\cos\theta,\qquad w=-\dot{e}\sin\theta, \tag{3}$$

where u, v and w are in x, r and θ directions respectively.

At the inlet of the fixed annular passage ($x=-l_0$), the inflow boundary conditions are defined by the nondimensional velocity components of fully developed laminar flow.

When the amplitude of oscillation is small compared to the annular space, the momentum equation in Eqs. (1) is written as

$$\frac{3\mathbf{V}^{n+1}-4\mathbf{V}^{n}+\mathbf{V}^{n-1}}{2\Delta t}+\mathbf{Q}^{n+1}=\mathbf{0}, \tag{4}$$

in which a three-point backward implicit scheme for the real time discretization is used. The solution at time level t^{n+1} has to be obtained from the equations

$$\mathbf{V}^{n+1}+\alpha\mathbf{Q}^{n+1}=\mathbf{F}^{n},\qquad \nabla\cdot\mathbf{V}^{n+1}=0, \tag{5,6}$$

where $\alpha=\frac{2}{3}\Delta t$, $\mathbf{F}^n=\frac{1}{3}(4\mathbf{V}^n-\mathbf{V}^{n-1})$ and Δt is the physical time step.

The solution of Eqs. (5) and (6) is obtained by using an iterative pseudo-time relaxation method with artificial compressibility (Soh and Goodrich, 1988).

An implicit Euler scheme is used to semi-discretize in pseudo-time the resulting equations. The final form of the momentum and continuity equations is obtained as

$$(\mathbf{I}+\Delta\tau)\Delta\mathbf{V}+\alpha\Delta\tau\Delta\mathbf{Q}=\Delta\tau\left(\mathbf{F}^n-\breve{\mathbf{V}}^v-\alpha\breve{\mathbf{Q}}^v\right), \quad (7)$$

$$\Delta p+\frac{\Delta\tau}{\delta}\nabla\cdot(\Delta\mathbf{V})=-\frac{\Delta\tau}{\delta}\nabla\cdot\breve{\mathbf{V}}^v, \quad (8)$$

where $\Delta\mathbf{V}=[\Delta u,\Delta v,\Delta w]^{\mathrm{T}}$, $\Delta\tau$ is the pseudo-time increment, δ is the artificial compressibility and $\Delta\mathbf{Q}=[\Delta Q_u,\Delta Q_v,\Delta Q_w]^{\mathrm{T}}$ in which $\Delta Q_u,\Delta Q_v$ and ΔQ_w are expressed, using lagged nonlinearities.

A factored ADI scheme (Soh, 1987) is used in this analysis to separate the numerical integration of Eqs. (7) and (8) in x, r and θ sweeps, which leads

$$(\mathbf{I}+\alpha\Delta\tau\mathbf{D}_x)(\mathbf{I}+\alpha\Delta\tau\mathbf{D}_r)(\mathbf{I}+\alpha\Delta\tau\mathbf{D}_\theta)\Delta\mathbf{f}=\Delta\tau\mathbf{R}, \quad (9)$$

where $\Delta\mathbf{f}=[\Delta u,\Delta v,\Delta w,\Delta p]^{\mathrm{T}}$, and $\mathbf{I}$ represents the unit matrix.

Equation (9) are factorized and further spatially discretized by central differencing, as mentioned before, on a stretched staggered grid based on hyperbolic stretching functions to concentrate more points near the oscillating and fixed boundaries. The final computational results at each real time step are Δu, Δv, Δw and Δp from which the values of unsteady u, v, w and p at time $n+1$ are obtained via

$$u^{n+1}=u^n+\Delta u, \qquad v^{n+1}=v^n+\Delta v,$$
$$w^{n+1}=w^n+\Delta w, \quad p^{n+1}=p^n+\Delta p;$$

they are the output of the numerical computation. It should be mentioned that the values obtained for these quantities are steady plus complex unsteady values. First, by using a sort of FFT program (Cooley et al., 1969), the amplitude and phase angle of each variable are determined and then the steady part is subtracted from the calculated value to obtain the unsteady part. For more details refer to Mekanik and Paidoussis, 2007.

FORCES ACTING ON THE CYLINDER AND STRUCTURAL EQUATION OF MOTION

The steady and unsteady forces are obtained by integrating the pressure and skin friction around the cylinder. Thus, the unsteady forces acting on the outer cylinder per unit length due to its oscillatory motion can be obtained as:

$$F(t)=\int_0^{2\pi}\left(\tau_{rr}|_{r=r_o}\mathrm{c}-\tau_{r\theta}|_{r=r_o}\sin\theta\right)r_o\sin\theta d\theta, \quad (10)$$

in which τ_{rr} and $\tau_{r\theta}$ are shear stresses.

The forces obtained from Eq. (10) are used in the equation of motion of the structure to analyze the dynamics and stability of the system. Hence, for translational motion of the outer cylinder one can write

$$M\ddot{y}+C\dot{y}+Ky=F(t), \quad (11)$$

where M,C, and K are mass, damping and stiffness of the moving cylinder respectively and y is the displacement of the cylinder after interaction with the fluid. Equation (11) is also nondimensionalized with respect to the annular gap h and the characteristic velocity U. The fluid force $F(t)$ is a function of $\varepsilon(t)$, $\dot{\varepsilon}(t)$, and $\ddot{\varepsilon}(t)$, as seen in Fig. 1, through the added stiffness, added damping and added mass effects, respectively.

To integrate Eq. (11) it is assumed at the beginning that the time level t^n has been reached, where all the quantities necessary to describe the structural motion are known: the displacement ε, and the velocity $\dot{\varepsilon}$, of the structure, and the fluid forces acting on it, $F(\varepsilon^n,\dot{\varepsilon}^n)\equiv F^n$. These quantities are known at all previous time levels t^k, $k\le n$, and the solution is advanced to t^{n+1}. For structural motion analysis, this is done using a second-order Runge-Kutta scheme in which a predictor step followed by a corrector step calculates the displacement as well as velocity and acceleration of the outer cylinder as a function of time. For more details refer to Mekanik 1993. It should be noted that all quantities in this method are nondimensionalized with respect to a reference velocity U_o and annular gap h.

SECOND METHOD

THE FLOW MODEL

The unsteady, compressible, Navier-Stokes equations for a 3-D flow can be cast in terms of absolute velocity **u** but solved in a relative non-Newtonian reference frame. This system of equations, written in an arbitrary Eulerian Lagrangian (ALE) conservative form for a control volume Ω with boundary Γ, takes the form

$$\frac{\mathrm{d}}{\mathrm{d}t}\int_\Omega \mathbf{U}\mathrm{d}\Omega+\oint_{\partial\Omega}\left(\boldsymbol{F}-\frac{1}{\mathrm{Re}}\mathbf{G}\right)\cdot\boldsymbol{n}\mathrm{d}\Gamma=0, \quad (12)$$

$\boldsymbol{n}$ represents the outward unit vector of the control volume boundary Γ. The viscous term **G** on the left-hand side of Eq. (12) has been scaled by the reference Reynolds number for nondimensionalization purposes. The solution vector of conservative variables **U** is given by

$$\mathbf{U}=\begin{bmatrix}\rho\\ \rho\mathrm{u}\\ \rho e\end{bmatrix}, \quad (13)$$

The inviscid flux vector **F** has the following components:

$$\mathbf{F} = \mathbf{U}\mathbf{v} + \begin{bmatrix} 0 \\ \rho\delta_{ij} \\ u_j \end{bmatrix}, \qquad (14)$$

where δ_{ij} represents the Kronecker delta function, u_j is the components of absolute velocity and $\mathbf{v}$ is the velocity in the relative frame of reference. The pressure p and the total enthalpy h are related to density ρ, absolute velocity $\mathbf{u}$ and internal energy e by two perfect gas equations:

$$p = (\gamma - 1)\rho[e - |\mathbf{u}|^2/2], \quad h = e + (p/\rho),$$

where γ is the constant specific heat ratio. The viscous flux vector **G** has the following components:

$$\mathbf{G} = \begin{bmatrix} 0 \\ \sigma_{ij} \\ \mu\sigma_{ij} + \frac{\gamma}{\gamma - 1}\left(\frac{\mu}{Pr}\right)\frac{\partial T}{\partial x_i} \end{bmatrix}. \qquad (15)$$

where x_i are the coordinates.

The viscous stress tensor σ_{ij} is expressed using the eddy viscosity concept which assumes that, in analogy with viscous stresses in laminar flows, the turbulent stresses are proportional to the mean velocity gradients:

$$\sigma_{ij} = \mu\left(\frac{\partial u_i}{\partial x_j} + \frac{\partial u_j}{\partial x_i}\right), \qquad (16)$$

μ represents the molecular viscosity given by the Sutherland's formula. The laminar Prandtl number, Pr_l, is taken as 0.7 for air.

NUMERICAL METHODOLOGY

The three-dimensional spatial domain is discretized using unstructured grids which, in principle, can contain cells with any number of boundary faces. The solution vector is stored at the vertices of the cells.

The present work uses semi-structured grids for their computational efficiency, although the solver is written for general hybrid unstructured grids. To achieve further computational efficiency, the mesh is represented using an edge base data structure. In this approach, the grid is presented to the solver as a set of node pairs connected by edges. The edge weights representing the inter-cell boundaries are computed in a separate pre-processor stage. Consequently, the solver has a unified data structure for which the nature of the hybrid mesh is concealed from the main calculation loops.

The flow model will now be explained in more detail. For clarity, the numerical discretization of the flow equations will be illustrated on a 2-D mesh. However, the resulting formulation is equally applicable to 3-D cells. Using an edge-based scheme, the typical 2-D mesh of Figure 2 can be discretized by connecting the median dual of the cells surrounding an internal node. For internal node I, the semi-discrete form can be written as

$$\frac{\mathrm{d}(\Omega_I \mathbf{U}_I)}{\mathrm{d}t} + \sum_{s=1}^{n_s} \frac{1}{2}\left|\eta_{IJ_s}\right|\left(\mathcal{F}_{IJ_s} - \mathcal{G}_{IJ_s}\right) + B_i = 0, \qquad (17)$$

where Ω_I is the area of the control volume (shaded area in Fig. 2), $\mathbf{U}_I$ is the solution vector at node I, n_s is the number of sides connected to node I, $\mathcal{F}_{IJ_s}$ and $\mathcal{G}_{IJ_s}$ are the numerical inviscid and viscous fluxes along side IJs, and B_i is the boundary integral. The side weight η_{IJ_s} is given by the summation of the two dual median lengths around the side times their normals. For example, the weight of the side connecting nodes I and J_1 is given by

$$\eta_{IJ_1} = -\eta_{J_1 I} = \overrightarrow{AB} + \overrightarrow{BC}. \qquad (18)$$

The resulting numerical scheme is second-order-accurate in space for tetrahedral meshes. For prismatic and hexahedral cells, the scheme is still second-order-accurate for regular cells with right angles. In the worst case of a highly skewed cell, the scheme will reduce to first-order accuracy (Essers *et al*. 1995).

NUMERICAL SOLUTION

Equation (17) can be expressed in the form

$$\frac{\mathrm{d}(\Omega_I \mathbf{U}_I)}{\mathrm{d}t} = \mathbf{R}(\mathbf{U}). \qquad (19)$$

A second-order implicit backward time integration of Eq. (19) can be expressed as

$$\frac{3(\Omega\mathbf{U})_I^{n+1} - 4(\Omega\mathbf{U})_I^n + (\Omega\mathbf{U})_I^{n-1}}{2\Delta t} = \mathbf{R}(\mathbf{U}^{n+1}), \qquad (20)$$

From now on the same approach used in the first method is followed which results in

$$\Omega_I^{n+1}\left(\frac{1}{\Delta\tau} + \frac{3}{2}\frac{1}{\Delta t}\right)\Delta\mathbf{U}_I + \frac{3\Omega_I^{n+1}\mathbf{U}_I^m - 4(\Omega\mathbf{U})_I^n + (\Omega\mathbf{U})_I^{n-1}}{2\Delta t} = \mathbf{R}^{m+1}, \qquad (21)$$

or

$$\left(\frac{\Omega_I^{n+1}}{\Delta\tau} + \frac{3}{2}\frac{\Omega_I^{n+1}}{\Delta t} - \mathbf{J}^m\right)\Delta\mathbf{U}_I = \mathbf{R}^m - \frac{3}{2}\frac{\Omega_I^{n+1}}{\Delta t}\mathbf{U}_I^m - \mathbf{E}_I^n, \qquad (22)$$

where $\mathbf{U}^m$ the mth approximation to $\mathbf{U}^{n+1}$ and

$$\mathbf{E}_I^n = \frac{4(\Omega\mathbf{U})_I^n - (\Omega\mathbf{U})_I^{n-1}}{2\Delta t}. \qquad (23)$$

The left-hand side of Eq. (22) contains a portion of the physical-time derivative in order to reduce the pseudo-time-step in regions of the flow where the ratio pseudo/physical time-step, $\Delta\tau/\Delta t$, becomes large (Melson *et al.* 1993).

Equation (22) is solved iteratively until the term $\Delta\mathbf{U}_I$ is driven to a specified small tolerance. Within this iteration level, a Jacobi sub-iteration procedure is performed to solve the linearized system of equations described by Eq. (22). Time accuracy is guaranteed by the outer iteration level where the time-step is fixed throughout the solution domain, while the inner iteration procedure can be performed using traditional acceleration techniques such as local time-stepping and residual smoothing (Sayma et al., 2000).

STRUCTURAL MODEL

For a linear structure, the dynamic analysis can easily be achieved by uncoupling the structural equations of motion by a coordinate transformation via the mode shape matrix. For the linear part of the system, the reduced modal equations can be solved by time- marching, with the modal matrix providing the link between the principal coordinates in the equation of motion (EOM) and the physical coordinates of the structure.

The mode shape vectors can then be interpolated onto the aerodynamic grid points at the start of the calculation. Although no further interpolation is required, the mesh is still moved at each time-step to accommodate the aeroelastic motion. Assuming, for the time being, that the structure is linear, the aeroelastic EOM can be written as

$$[\mathbf{M}]\{\ddot{\boldsymbol{x}}\} + [\mathbf{C}]\{\dot{\boldsymbol{x}}\} + [\mathbf{K}]\{\boldsymbol{x}\} = \{p(t)\boldsymbol{n}\}, \tag{24}$$

where $\boldsymbol{n}$ is the normal unit vector on the cylinder surface.

The free vibration problem can be solved to yield natural frequencies, ω_i, and the mass-normalized mode shape matrix $[\boldsymbol{\Phi}]$. The required coordinate transformation is

$$\{\boldsymbol{x}\} = [\boldsymbol{\Phi}]\{\boldsymbol{q}\}, \tag{25}$$

where $\boldsymbol{q}$ is the vector of the principal or modal coordinates. Using Eqs. (24) and (25) and pre-multiplying by $[\boldsymbol{\Phi}]^{\mathrm{T}}$ yields

$$\begin{aligned}[\boldsymbol{\Phi}]^{\mathrm{T}}[\mathbf{M}][\boldsymbol{\Phi}]\{\ddot{\boldsymbol{q}}\} + [\boldsymbol{\Phi}]^{\mathrm{T}}[\mathbf{C}][\boldsymbol{\Phi}]\{\dot{\boldsymbol{q}}\} + [\boldsymbol{\Phi}]^{\mathrm{T}}[\mathbf{K}][\boldsymbol{\Phi}]\{\boldsymbol{q}\} \\ = [\boldsymbol{\Phi}]^{\mathrm{T}}\{p(t)\boldsymbol{n}\}.\end{aligned} \tag{26}$$

The structural equations of motion can be reduced further by removing both the coordinates and modes that are of no interest in the flutter calculations. Assuming proportional damping (without loss of generality) and using the orthogonality properties of the system matrices with respect to the mode shape matrix, one obtains

$$\begin{aligned}\{\ddot{\boldsymbol{q}}\}_N + [\mathrm{diag}(2\zeta_i\omega_i)]_{N\times N}\{\dot{\boldsymbol{q}}\}_N + [\mathrm{diag}(\omega_i^2)]_{N\times N}\{\boldsymbol{q}\}_N \\ = [\boldsymbol{\Phi}]^{\mathrm{T}}{}_{m\times N}\{p(t)\}_m = [\textstyle\prod(t)]_N,\end{aligned} \tag{27}$$

where ω_i and ζ_i are the natural frequency and modal damping for mode i, N is the number of structural coordinates and m is the number of modes. The right-hand-side vector of modal forces is formed as follows:

$$\textstyle\prod(t) = [\boldsymbol{\Phi}]^{\mathrm{T}}\{p(t)\boldsymbol{n}\} = \left\{\left(\sum_{i=1}^{n_a} p_i \emptyset_{i,r}\right).\boldsymbol{n}_i\right\}_{r=1,m}, \tag{28}$$

where n_a is the number of aerodynamic nodes on the structure surface.

In this form, the equations of motion can be solved by any standard numerical integration scheme and the self-starting, second-order-accurate and unconditionally stable Newmark discretization (Newmark 1959) was used in the current work.

MESH MOVEMENT

When undertaking a forced response aeroelasticity analysis, it is desirable to move the fluid mesh according to the instantaneous position of body under consideration so that the structure vibration can be included in the calculations. This requirement is met by using an algorithm which considers the mesh as a network of springs whose extension/compression is prescribed by the mode shape at the structure surface and becomes zero at the far field. At each node, the spring stiffnesses are allocated values that are inversely proportional to the length of the shared edge lengths. The CFD algorithm used in SURF takes full account of the unsteady fluxes which arise due to cell volume changes at each time-step.

SURF PACKAGE

In the second method a Code called SURF based on the above formulations is used to analyze the problem at hand.

The SURF Code is a suit of unsteady flow and aeroelasticity programs in which a typical analysis procedure involves five steps: mesh generation, pre-processing, mode shape interpolation, aeroelasticity computation and post-processing [SURF, V1.0, User Guide, Oct. 2007]. Each step can be performed by a single program or by a combination of programs incorporated in SURF. The mesh generated by SURF-Mesh is mostly used for turbomachinery analyses, but the meshes generated using most known commercial tools such as GAMBIT can be converted to SURF format using a functionality built in SURF-Toolbox. In the problem described in this paper, the general structured meshes are imported from grid generator GAMBIT.

ADAPTING THE METHODOLOGY TO ANNULAR FLOW PROBLEMS

For the first time the methodology related to the turbomachinery analysis and mentioned in the previous sections is used to analyze the annular flow-induced vibration problems. It is obvious that some of the physical characteristics of the flow in turbomachinery are not the same as their counter parts in the annular flows. For example, there is no reference frame rotating with the cylinders with circular frequency ω in annular flows as compared to the cases of the blades in turbomachines. Also, in the case of annular flows there is no need to use the unstructured grids to solve the fluid flows. Another simplification made to the above analysis is that since laminar flows are considered here, the turbulent's terms used in the turbumachinery analysis are not used in the present work.

The implicit temporal discretization used in the above analysis is almost the same as the discretization used in the first method described above and the boundary conditions used are much more simplified than that used for turbomachinery (see Sayma et al., 2000). In the structural model as shown in Eq. (24), only the pressure is considered *vis-à-vis* to the first method, (Eq. 11), in which the shear stresses are also taken into account.

RESULTS OF THE FIRST METHOD

A satisfactory grid generation and grid point distribution are the major requirements for the numerical solution to be accomplished successfully in terms of accuracy and stability. To this end, the numerical computations have been performed on a non-dimensional mesh for the annulus and $0 \le \theta \le \pi$, with $89 \times 12 \times 15$ grid points in the x, r, and θ directions, respectively and also stretched in x and r directions.

The computation can be done for different Reynolds and Stokes numbers (also defined as $S = \omega \mathrm{Re}_{D_h}/2$, which is related to the vibrational characteristics of the system) always in the laminar regime. For all of the results obtained in this work, the time step $\Delta t = T/N$ with $N = 19$ and the compressibility factor δ and pseudo-time step $\Delta\tau$ were chosen based on the criteria supplied by Soh and Goodrich 1988 and Chorin 1967. For the Courant-Friedrich-Levy (CFL) number, an average value between 30 and 40 has been considered. In all computations, convergence was reached and the iterations were stopped in pseudo-time when the r.m.s. values of the numerical residuals of the momentum and continuity equations were all less than 10^{-4}.

RESULTS FOR PRESCIPED OSCILLATORY MOTION

Figure 3(a,b) presents the unsteady pressure amplitude and phase angle versus the axial length of the cylinder obtained for 3-D solution of an annular passage, at $r = 9.965$ (close to the outer cylinder) and $\theta = 7.5^o$(azimuthal angle from the vertical line in Fig. 1). Since for the force calculation as shown in Eq. (10) we need the shear stresses on the outer cylinder, thus Fig. 4(a,b) presents the circumferential velocity w and its phase angle obtained at $X = 50$ (along the cylinder length) and $\theta = 45^o$. Figure 5 shows the displacement of the oscillating cylinder as a function of Reynolds number, for a system with $r_i = 9$ and $r_o = 10$. From Fig. 5, we see that at very low Reynolds number, $\mathrm{Re}_{D_h} = 4$, viscosity dominates the solution and motion is so highly damped that no oscillations are possible: the system is overdamped. As the Reynolds number increases, $\mathrm{Re}_{D_h} = 200$, damped oscillation develops. As the Reynolds number becomes larger, $\mathrm{Re}_{D_h} = 2000$, the viscous solution gets closer to the potential (inviscid) flow solution (also shown in the figure), i.e., zero dissipation, and hence zero fluid damping (Mateescu and Paidoussis 1985).

SPECIFICATIONS USED FOR SECOND METHOD

For this method, the geometrical specifications used for the annular geometry shown in Fig. 1 remain the same except that it is assumed that the outer cylinder is a continuous cylinder and there are no separated cylinders at the upstream and downstream ends of it. The dimensions of the system also remain the same. The mesh was generated using GAMBIT for this annular geometry and was fed into SURF for further modification and recognition by using SURF-Toolbox. The number of grid points used in r, θ and z directions are 10x200x100. We have four boundary conditions; the inlet and outlet boundaries with specified initial flow variables and the outer cylinder with specified modes of vibration. The inner cylinder, the fourth boundary, is assumed to remain stationary during computations. The fluid used was air with $p_{in} =$ 70002 pa, $p_{out} = 70000$ pa, $U_{in} = 0.5$ m/s, $U_{out} = 0.5$ m/s, $T_{in} = 285.0^o$ K and $T_{out} = 285.0^o$ K all at the beginning of the steady state computations. First, the steady state solution was obtained using SURF solver and then the unsteady solution is obtained by considering the modal motions of the outer cylinder. It is assumed that the upstream and downstream ends of the cylinder are stationary and the middle section which is 40 cm long is vibrating according to Eq. (29), (James et al., 1989):

$$y(z,t) = \varphi(z)q(t), \tag{29}$$

in which $\varphi(z)$ is a function of the spatial coordinate z and $q(t)$ is a function of time t. The function $\varphi(z)$ which shows the modal displacement of the cylinder is given by Eq. (30) assuming that the cylinder is treated as an Euler's beam with free-free ends:

$$\varphi_i(z) = \cosh k_i z + \cos k_i z - \alpha_i(\sinh k_i z + \sin k_i z), \tag{30}$$

in which $\alpha_i = (\cosh k_i l - \cos k_i l)/(\sinh k_i l - \sin k_i l)$, i is the mode number, z is the axial coordinate and l is the length of the vibrating part of the cylinder. As an example, for the first mode, $k_1 l = 4.730041$ and $\alpha_1 = 0.982502$. It is assumed that the cylinder is made from aluminum with the mass of $m =$ 10 kg and vibrating frequency given by $f = \omega/2\pi = l^2/(2\pi \times 22.373\sqrt{\frac{EI}{\gamma}}) = 32.15$ Hz for the first mode. We assume, for the time being, that the structural damping is zero. The modal motions was mass normalized according to Eq. (31), (James et al. 1989):

$$\varphi_{\text{normalized}} = \frac{\varphi(z)}{\mathrm{N.F.}}, \tag{31}$$

with

$$\mathrm{N.F.} = \sqrt{m\varphi(z_i)^2} \qquad i = 1, \cdots 100, \tag{32}$$

in which i indicates the node number of the outer cylinder's mesh along z axis.

For unsteady solution, in the input file of the mode shape, the initial velocity for the outer cylinder was assumed to be $0.1\ \mathrm{m}\sqrt{\mathrm{kg}}/\mathrm{s}$ with its initial displacement and acceleration equal zero.

To obtain a converged solution, both for steady and unsteady cases, the CFL number was assumed to change from 0.5 to 30. The number of time-step for convergence was chosen to be 4000 with $\Delta t = 0.01$ sec by which the residual of the continuity equation became of order of 10^{-4}

RESULTS OF THE SECOND METHOD

Based on the specifications and formulations mentioned in the previous sections, and for Re = 175 with $w = 0.1941\ \mathrm{m/s}$, $\rho = 0.855\ \mathrm{kg/m^3}$, $\mu = 1.9 \times 10^{-5}\mathrm{N-s/m^2}$ and hydraulic diameter $D_H = 2h = 0.02$ m, the following results have been obtained. Figure. 6 shows the mesh generated by GAMBIT and used in SURF. It is seen that the mesh is structured one used in this analysis. The outer meshed cylinder is moving during the vibration analysis with for example the first mode shape shown in Fig. 7. All the following figures were obtained at the last time step where the program converged to the final solution. As shown in Fig. 8, for the points on the central part of the cylinder which are vibrating, the pressure generated fluctuates with time for longer time steps. In Fig. 9 the variation of the force from the fluid imposed on the cylinder is shown. This force is obtained by integration of the unsteady pressure (Fig. 8) over the surface of the outer cylinder. Figure 10 presents the displacement of the outer cylinder in x-direction for the first mode. This figure is a kind of flutter motion and the effect of the damping from the fluid on the annular system due to the vibration of the outer cylinder is shown in this figure. By using the logarithmic decrement one can obtain the damping factor related to the damping introduced into the system. Figure 11 demonstrates the behavior of the outer cylinder when the second mode was used as forcing function in structural equation. As shown in this figure, the motion of the cylinder is also damping out due to the added damping introduced into the system by the fluid but the rate is more than that for the first mode. Finally, Fig. 12 shows the response of the structure during the third mode vibration. It seems that the cylinder diverges after a few oscillations but finally it flutters with almost constant amplitudes.

CONCLUSIONS

In this paper, two accurate methods have been applied to study the annular flow-induced instabilities.

The first method uses the small amplitude motion of the outer cylinder to analyze the problem considered by using the direct coupling of the fluid and structure equations. In this method the time-integration of the incompressible laminar Navier-Stokes (N-S) and continuity equations was effected by using the method of artificial compressibility in conjunction with a three-point backward implicit real-time differencing scheme.

The theoretical results obtained predict the behaviour of the structure (the outer cylinder) when it is set in motion from rest. The stability of the system was analyzed for three-dimensional annular flows with uniform annular geometry and translational oscillation of the outer cylinder. It was shown that the outer cylinder is more stable when the Reynolds number is not very large (in the laminar regime), and that as Re becomes larger the system becomes less stable. The results obtained for uniform annular viscous flow indicate the generation of a viscosity-related added damping (which is not present for potential flow). Therefore the following points deserve consideration:

(i) The damping forces and pressure distribution along the annulus can be well predicted if simple assumptions about the unsteady flow in the annulus are made.

(ii) The flow-induced damping (velocity-dependent) and stiffness (displacement-dependent) forces acting on the oscillatory and non-oscillatory walls.

(iii) The uniform annulus results demonstrate the generation of a negative fluid-stiffness force for the lateral motions in the annulus. If the restoring (positive) spring stiffness is sufficiently small, then, for a given flow velocity, the overall stiffness may vanish, giving rise to static (divergence) instability.

In the second method use is made of the SURF Code and its Tool Boxes, which are developed to analyse the turbo-machinery problems, for both laminar and turbulent flows. In this Code, the Navier-Stokes equations are used to represent the unsteady flow in a nonlinear time-accurate fashion. The structural model is based on a linear modal model. The fluid mesh is moved at each time-step according to the structural motion, so that the changes in aerodynamic damping and flow unsteadiness can be accommodated. In this way the stability analyses can be performed for the structure.

By this approach, in addition to the results which can be obtained for, density, pressure, velocity, temperature and other variables of the flow, one can assess the stability of the structure through vibrational analysis. Thus, the results obtained indicate that the annular flow system considered becomes stable due to the positive damping introduced in the system by the fluid for the first and second modes and unstable for the third mode which may result in flutter motion.

The important features of the second method which can be used for the future extension of the present work, and also are not existed in the first method are:

(i) can be used to analyse the stability of the structure along different direction of the coordinate axes.

(ii) can handle several modes of vibration of the structure

(iii) can handle the turbulent flows.

(iv) can be used for different geometrical annular shapes

REFERENCES

Chorin A.J. 1967. A numerical method for solving incompressible viscous flow problems. Journal of Computational Physics 2, 12-26.

Cooley, J.W., Lewis, P.A.W., Welch, P.D., 1969. The Finite Fourier Transform. IEEE Transactions on Audio and Electronics, AU-17, 77-85.

Essers, J. A., Delanaye, M. and Rogiest, P., 1995. Upwind-biased finite-volume technique solving Navier-Stokes equations on irregular meshes. *AIAA Journal* **33**, 833-842.

James, M. L., Smith, G. M., Wolford, J. C. and Whaley, P. W., 1989. Vibration of Mechanical and Structural Systems with Microcomputer Applications. Harper and Row Publishers, New York.

Mateescu, D. and Paidoussis, M. P., 1985. The unsteady potential flow in an axially variable annulus and its effect on the dynamics of the oscillating rigid centre-body. Journal of Fluids Engineering 107**,** 421-427.

Mateescu, D. and Paidoussis, M. P., 1987. Unsteady viscous effects on the annular-flow-induced instabilities of a rigid cylindrical body in a narrow duct. *Journal of Fluids and Structures* 1**,** 197-215.

Mateescu, D., Paidoussis, M. P. and Belanger, F., 1988. Unsteady pressure measurements on an oscillating cylinder in narrow annular flow. *Journal of Fluids and Structures* **2**, 615-628.

Mateescu, D., Paidoussis, M. P. and Belanger, F., 1991. Computational Solutions Based on a Finite Difference Formulation for Unsteady Internal Flows, AIAA Paper No. 91-0724.

Mateescu, D., Païdoussis, M. P. and Bélanger, F., 1994a**.** Unsteady annular viscous flows between oscillating cylinders. Part I: Computational solutions based on a time-integration method. *Journal of Fluids and Structures,* Vol. **8,** 1994, pp. 489-507.

Mateescu, D., Païdoussis, M. P. and Bélanger, F., 1994b**.** Unsteady annular viscous flows between oscillating cylinders. Part II: A hybrid time-integration solution based on azimuthal Fourier expansions for configurations with annular backsteps. *Journal of Fluids and Structures* **8,** pp. 509-527.

Mateescu, D., Païdoussis, M. P. and Bélanger, F., 1994c**.** A time-integration method using artificial compressibility for unsteady viscous flows. *Journal of Sound and Vibration* 1**77,** No. 2, pp. 197-205.

Mekanik, A., Mateescu, D. and Païdoussis, M.P., 1993, Computational Solution of Navier-Stokes Equations for Annular Flows with Moving Boundaries. pp. *243-244, Proceedings of* 14lh *Canadian Congress of Applied Mechanics,* Queen's University, Kingston, Ont., Canada.

Mekanik, A. and Paidoussis, M. P., 2007. Stability analysis of uniform and non-uniform annular passages conducting incompressible laminar flows for small and large amplitude oscillatory motions of the outer cylinder. *Journal of Sound and Vibration*, 2007, 303, 78-108.

Melson, N. D., Sanetrik, M. D. and Atkins, H. L., 1993. Time-accurate Navier-Stokes calculations with multigrid acceleration. *Proceedings of the Sixth Copper Mountain Conference on Multigrid Methods*.

Newmark, N. M., 1959. A method of computation for structural dynamics. *ASCE Journal of Engineering Mechanics Division* **8**, 67-94.

Païdoussis, M.P., 1998. Fluid-Structure Interactions, Slender Structures and Axial Flow. Vol. 1, Academic Press, London.

Païdoussis, M.P., 2003. Fluid-Structure Interactions, Slender Structures and Axial Flow. Vol. 2, Elsevier Academic Press, London.

Parking, M. W. and Watson, P. C., 1984. Reduction of vibration caused by flow in an annular diffuser. ASME Symposium on Flow-Induced Vibrations, Volume 4, 1-14.

Sayma, A. I., Vahdati, M. and Imregun, M., 2000. An Integrated nonlinear approach for turbomachinary forced response prediction. Part I: Formulation. *Journal of Fluids and Structures* 14**,** 87-101.

Soh, W.Y., 1987. Time-marching solution of incompressible Navier-Stokes equations for internal flows. Journal of Computational Physics 70, 232-252.

Soh, W.Y., Goodrich, J.W., 1988. Unsteady solution of incompressible Navier-Stokes equations. Journal of Computational Physics 79, 113-134.

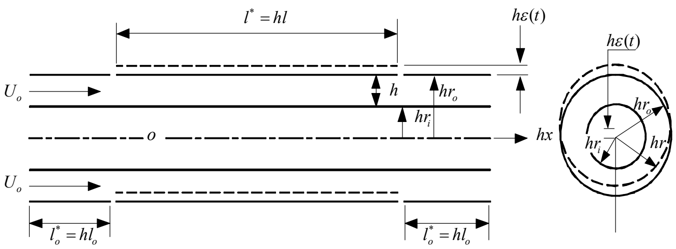

Figure 1. Geometric representation of uniform annular passage with oscillating middle section of the outer cylinder.

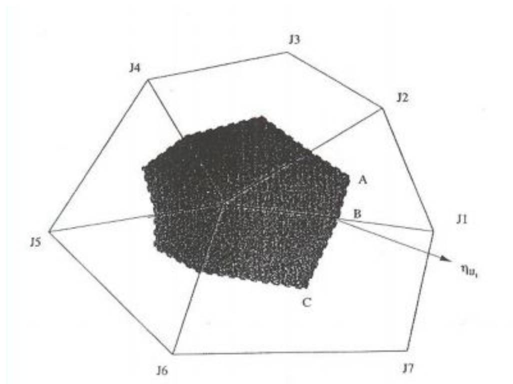

Figure 2. Typical 2-D mixed-cell mesh.

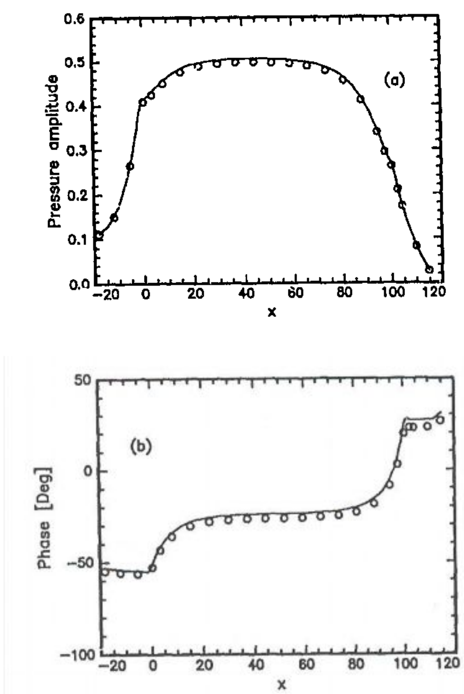

Figure 3: The unsteady pressure (a) and phase angle (b) for Re = 250, $\omega = 0.2$, $r_i = 9$, $r_o = 10$ at $r = 9.965$, $\theta = 7.5^o$and $\epsilon = 0.1$.

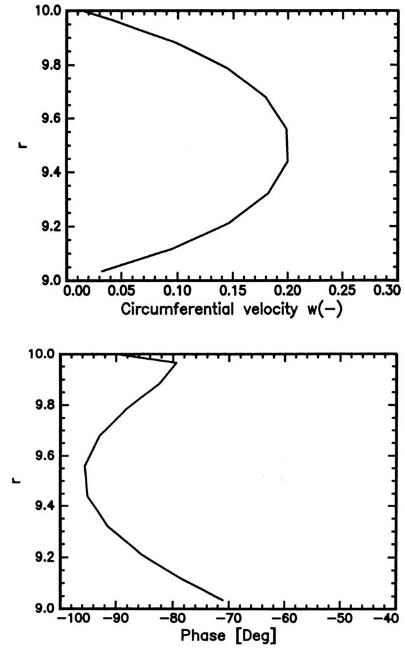

Figure 4: (a) The circumferentia1 velocity w and (b) phase angle with respect to the displacement of the outer cylinder in annular gap for Re =250, $\omega = 0.2$, $r_i = 9$, $r_o = 10$, and f = 0.1 at $X = 50$, $\theta = 45^o$.

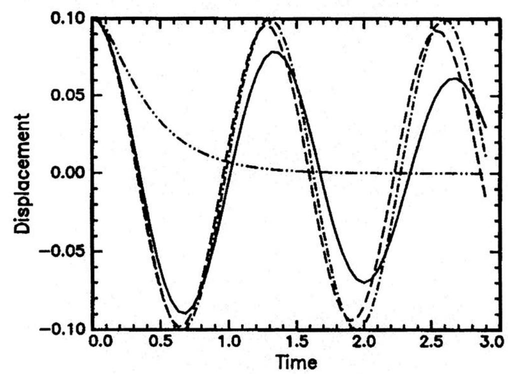

Figure 5. Displacement, ε, of the outer cylinder in translational motion versus time, $T_n = 2\pi/\omega_n$, with $\omega_n = 1$ for a 2-D annulus ;–··–··–, $\mathrm{Re}_{D_h} = 4$;——, $\mathrm{Re}_{D_h} = 200$;– – – , $\mathrm{Re}_{D_h} = 2000$;–·–·– , potential flow.

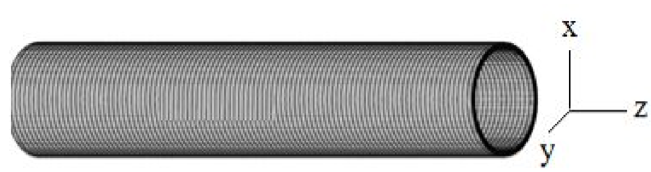

Figure 6. Mesh generated for the annulus. 10x200x100 in r, θ and z-directions. The $r_i = 9$, $r_o = 10$ and the length of the cylinder is 100 cm. The middle 40 cm of the outer cylinder is oscillating.

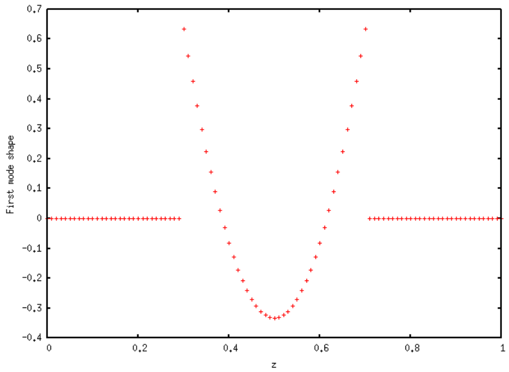

Figure 7. The first mode shape for the outer pipe.

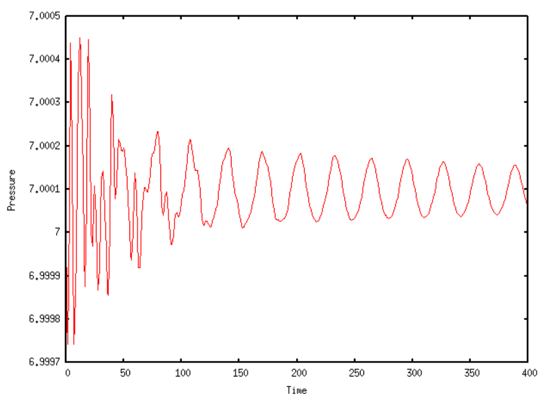

Figure 8. Pressure fluctuation at $x = -0.1$, $y = 0.0$ and $z = 0.54$ due to the oscillation of outer cylinder.

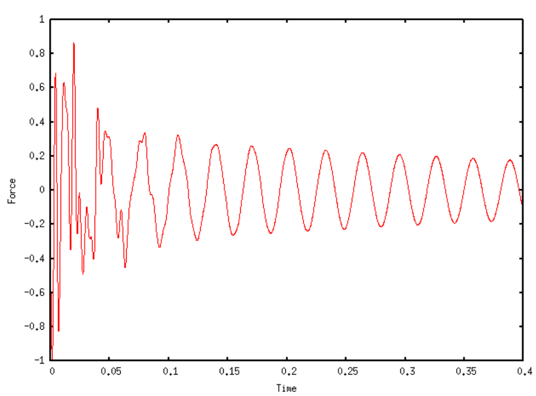

Figure 9. Force acting on the cylinder due to the unsteady pressure versus time.

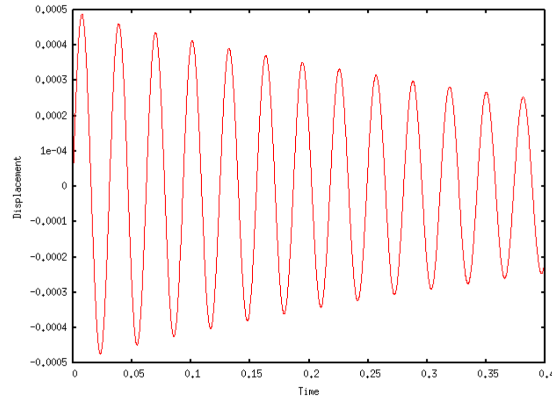

Figure 10. Displacement of the outer cylinder in x-direction versus time, first mode.

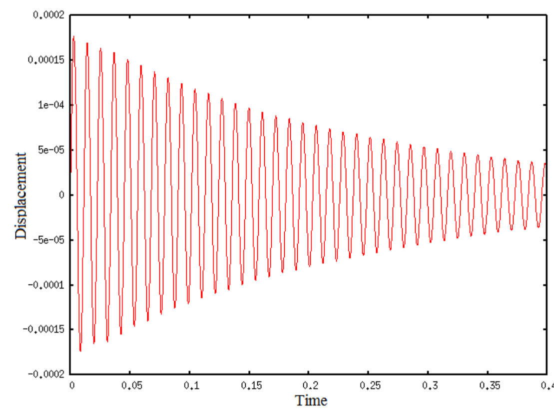

Figure 11. Displacement of the outer cylinder in x-direction versus time, second mode.

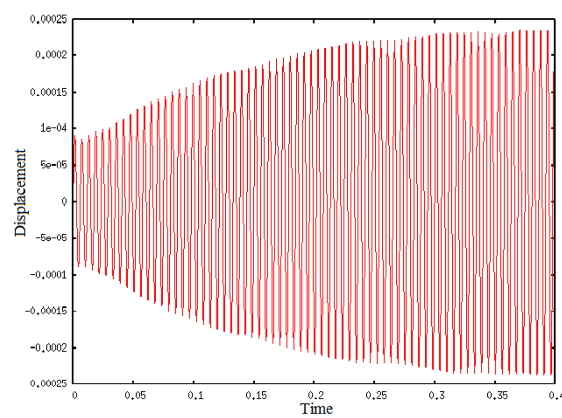

Figure 12. Displacement of the outer cylinder in x-direction versus time, third mode.